Published in final edited form as:
Science. 2019 June 07; 364(6444): 987–990. doi:10.1126/science.aav7617.

Prenatal activity from thalamic neurons governs the emergence of functional cortical maps in mice

Noelia Antón-Bolaños[#1], **Alejandro Sempere-Ferràndez**[#1], **Teresa Guillamón-Vivancos**[1], **Francisco J. Martini**[1], **Leticia Pérez-Saiz**[1], **Henrik Gezelius**[1,2], **Anton Filipchuk**[1,3], **Miguel Valdeolmillos**[1], **Guillermina López-Bendito**[1,*]

[1]Instituto de Neurociencias de Alicante, Universidad Miguel Hernández-Consejo Superior de Investigaciones Científicas (UMH-CSIC), Sant Joan d'Alacant, Spain

[#] These authors contributed equally to this work.

Abstract

The mammalian brain's somatosensory cortex is a topographic map of the body's sensory experience. In mice, cortical barrels reflect whisker input. We asked whether these cortical structures require sensory input to develop or are driven by intrinsic activity. Indeed, thalamocortical columns, connecting thalamus to cortex, emerge before sensory input and concur with calcium waves in the embryonic thalamus. We show here that the columnar organization of the thalamocortical somatotopic map exists in the mouse embryo before sensory input, thus linking spontaneous embryonic thalamic activity to somatosensory map formation. Without thalamic calcium waves, cortical circuits become hyperexcitable, columnar and barrel organization do not emerge, and the somatosensory map lacks anatomical and functional structure. Thus, a self-organized protomap in the embryonic thalamus drives functional assembly of murine thalamocortical sensory circuits.

The mammalian cerebral cortex is arranged into radial columns that coalesce during development. These columns become functionally organized before adulthood (1–3). Some evidence suggests that genetic factors regulate initial columnar patterning (4); other evidence suggests functional maps arise postnatally as a result of sensory experience (5–9). However, spatially organized patterns of spontaneous activity are evident in the embryonic thalamus, before cortical neurons have completed their radial migration (10). One well-studied functional map is the somatotopic correspondence between whiskers and their associated clusters of layer 4 neurons (called barrels) in the rodent primary somatosensory cortex (S1) (11). Although barrels are apparent anatomically at postnatal day 4 (P4) (12), domains of

[*]**Address correspondence to: g.lbendito@umh.es**.
[2]Present address: Science for Life Laboratory, Tomtebodavägen 23A, 17165 Solna, Sweden.
[3]Present address: Department of Integrative and Computational Neuroscience (ICN), Paris-Saclay Institute of Neuroscience (NeuroPSI), CNRS/University Paris-Sud, 91198 Gif-sur-Yvette, France.

Author contributions: N.A-B, A.S-F, M.V and G.L-B designed the experiments. N.A-B, A.S-F, T.G-V, FJ.M and L.P-S performed the analysis; N.A-B conducted calcium imaging, tracing experiments, and the cFos assays. A.S-F conducted calcium imaging and the electrophysiology. T.G-V conducted the *in vivo* calcium imaging. FJ.M performed the Matlab analysis. L.P-S and FJ.M performed the *in vivo* multi-electrode recordings. H.G generated the Kir-mCherry mouse and pioneered Th^{Kir} analysis. A.F designed, performed and analyzed initial spontaneous thalamic calcium imaging. G.L-B acquired funding; and M.V and G.L-B wrote the paper.

Competing interests: None declared.

Europe PMC Funders Author Manuscripts

spontaneously co-activated neurons can be identified at birth in S1 *in vivo* (13–15). We asked whether the emergence of anatomically discernable structures is preceded by organized activity in the mouse embryo. We discovered that structured patterns of neuronal activity in the embryonic thalamus define functional cortical columns and the concomitant functional somatotopic map in the immature cortex.

The functional properties of embryonic thalamocortical connections were assessed by recording the somatosensory cortical calcium responses elicited by the activation of the ventral postero-medial nucleus (VPM) of the thalamus in slices. By embryonic day 17.5 (E17.5), electrical stimulation of the VPM triggered calcium waves that propagated over a large area of the nucleus, resembling previously reported spontaneous activity (10). This thalamic stimulation elicited a cortical calcium response in the S1 (Fig. 1A and B, fig. S1A; movie S1). While activation of thalamocortical axons is confined to the subplate at this stage (fig. S1B), the cortical response spanned the entire thickness of the cortical plate, suggesting that thalamocortical axons activate a radially organized cortical network. From E18.5 onwards, VPM stimulation activated a progressively restricted territory within the nucleus (fig. S1C), allowing us to define the functional topography of the nascent thalamocortical projection. Peri-threshold stimulation of adjacent regions in the VPM activated distinct columnar territories in the cortex (Fig. 1, C and D), indicating the existence of a functional protomap present in these embryonic thalamocortical circuits. This was evaluated *in vivo* by transcranial calcium imaging of glutamatergic cortical neurons at E18.5. Mechanical stimulation of juxtaposed areas of the whisker pad activated discrete, segregated and spatially consistent cortical territories in the contralateral S1 (Fig. 1, E and F; movie S2), confirming the existence of a cortical somatosensory protomap in the intact embryo.

We then tested whether embryonic thalamic calcium waves influence the emergence of the functional cortical columns that presage the formation of the somatotopic barrel map. To change the normal pattern of spontaneous thalamic activity, we crossed a tamoxifen-dependent *Gbx2Cre^{ERT2}* mouse with a floxed line expressing the inward rectifier potassium channel 2.1 (Kir) fused to the mCherry reporter (fig. S2) (10). In this model (*Th^{Kir}* hereafter), 78% of the VPM neurons express Kir-mCherry protein upon tamoxifen administration at E10.5 (fig. S2). In control slices, more than half of the spontaneous synchronous events in the VPM corresponded to large amplitude-highly synchronized calcium waves, whereas the remaining activity reflected low amplitude, poorly synchronized events. The highly synchronized waves were not detected in the *Th^{Kir}* mice, in which only small amplitude and mostly asynchronous activity persisted, although at a higher frequency than in controls (Fig. 2, A-C; movies S3 and S4). Collectively, Kir overexpression shifted the pattern of spontaneous activity in the thalamus from synchronized waves to asynchronous activity.

At the cellular level, while control neurons were relatively depolarized at E16.5, *Th^{Kir}* cells displayed a bi-stable pattern of activity with spontaneously alternating periods of hyperpolarized and depolarized membrane potential (Fig. 2D and fig. S3). Action potentials were generated in the depolarized phase in both control and *Th^{Kir}* cells. This change in the electrical properties of the *Th^{Kir}* neurons was sufficient to impede the generation of calcium waves. Indeed, barium, an ion that blocks Kir channels (16), reversed the

electrophysiological profile of Th^{Kir} neurons, recovering the wave-like activity in Th^{Kir} VPM networks (fig. S4 and movie S5). Thus, while there were no propagating calcium waves in the thalamus of Th^{Kir} mice, the preservation of its asynchronous activity meant it was not silent.

We analyzed how altering the pattern of spontaneous thalamic activity in our Th^{Kir} model affected the functional columnar organization in S1. Peri-threshold VPM stimulation in E17.5-E18.5 slices from control mice triggered a columnar-like cortical response (fig. S5A and movie S6). Conversely, this stimulation in Th^{Kir} slices consistently elicited a broader (laterally) cortical calcium wave (fig. S5A; movies S7 and S8). Despite these differences, the subplate was the earliest cortical compartment activated in both control and T^{Kir} mice, followed by the upper cortex (fig. S5, B-D). Next, we tested whether the emergence of the functional topographic map was affected in the Th^{Kir} mice. Unlike the controls, stimulation of adjacent regions in the VPM in the Th^{Kir} slices activated highly overlapping territories in the cortex (Fig. 3A), indicating that the topographical representation of the thalamocortical circuit does not emerge in the absence of embryonic thalamic waves. Postnatally, the cortical response to VPM stimulation narrowed progressively with time in control slices, coinciding at P4 with the dimensions of the cortical barrel, yet this spatial restriction occurred to a lesser extent in the Th^{Kir} mice (Fig. 3, B and C; movies S9 and S10). These differences were observed irrespective of the stimulation strength (fig. S6).

The extended cortical activation in the Th^{Kir} mice was not due to more extensive activation of the VPM (fig. S7), yet it was associated with increased levels of intrinsic cortical excitability. This was reflected by the high frequency of spontaneous cortical waves in Th^{Kir} slices (fig. S8, A and B) and the widespread cortical response to intracortical stimulation (fig. S8, C-E). Next, we tested whether this change in cortical network excitability occurred in the Th^{Kir} mice *in vivo*. Because cortical travelling waves were associated with action potentials bursts (fig. S8F), we recorded extracellular cortical activity with multichannel electrodes. We found extensive spontaneous events of synchronous activity spreading horizontally in the Th^{Kir} mice at P2-P3 (Fig. 3, D-F), consistent with the hyperexcitability observed *ex vivo*. Then, we analyzed the possible origin for this excitability and found that the amplitude of the calcium response was the same in the subplate but larger in the upper cortex in the Th^{Kir} mice (fig. S9), suggesting a local alteration in the upper cortical network. As metabotropic glutamate receptors (mGluRs) participate in the propagation of cortical spontaneous activity in newborn rodents (17, 18), we tested whether mGluRs could be involved in the hyperexcitability of cortical networks in Th^{Kir} mice. Bath application of MPEP (100 μM), a mGlu5 specific antagonist, rescued the activation of the thalamocortical-induced cortical network into a column-like domain in Th^{Kir} mice. Albeit MPEP decreased the overall signal intensity in both conditions, it had no effect in the width of the cortical response in controls (fig. S10, A-C). These results are consistent with increased expression of cortical mGlu5 in the Th^{Kir} mice at P0 (fig. S10D). Together, these data reveal that the emergence of functional columns and somatotopic map in the S1 relies on thalamic control of cortical excitability, implicating mGluRs.

To ascertain whether embryonic thalamic activity and functional columns are a pre-requisite to establish the postnatal anatomy of the barrel map, we examined thalamocortical axons

clustering in the Th^{Kir} mice in which this projection was labelled by GFP (19). The barrel map was evident at P4 in control mice (12, 20) but no barrels were detected in tangential or coronal sections of Th^{Kir} mice, where thalamocortical axons targeted the layer 4 but did not segregate into discrete clusters (Fig. 4A and fig. S11). Furthermore, there was no arrangement of layer 4 cells into barrel walls in the Th^{Kir} mice. The absence of barrels did not seem to originate from the loss of neurotransmitter release (*21, 22*), as thalamic neurons in the Th^{Kir} fire action potentials and activate synaptic currents in cortical cells (fig. S4A, S9D and S12, A-C), and respond normally to whisker stimulation *in vivo* (fig. S12, D and E).

The disrupted barrel map in Th^{Kir} mice could reflect altered point-to-point connectivity at several subcortical levels (8, 23, 24). However, the organization of brainstem barrelettes and thalamic barreloids in the Th^{Kir} mice was normal (fig. S13). Since the barrel map ultimately relies on the specific topographic organization of thalamocortical axons (25), we explored whether some spatial segregation was conserved in the Th^{Kir} mice. While dye deposition in barrels C1 and C4 back-labeled cells in the corresponding barreloids of control mice, the back-labeled territories in Th^{Kir} mice were more extensive, including cells located in neighboring barreloids (Fig. 4, B and C). Anterograde tracing from single barreloids also revealed a broader horizontal disposition of thalamocortical axons in the layer 4 of the Th^{Kir} mice (fig. S14). Finally, we determined how this aberrant topographic map generated by the lack of thalamic calcium waves affected the relay of sensory stimuli in early postnatal mice *in vivo*. While stimulation of distinct points on the whisker pad at P3-P4 activated discrete barrel-like patches in the control S1, similar stimulations of Th^{Kir} mice led to enlarged responses in the barrel-field (Fig. 4D; movies S11 and S12). Together, these data demonstrate that the postnatal anatomic clustering of thalamocortical axons and the somatotopic functional map is disrupted in the absence of embryonic thalamic waves.

As the critical period of thalamocortical plasticity in the S1 closes between P3 and P7 in rodents (6, 20, 26), we assessed whether the loss of columnar organization in the Th^{Kir} mice could be overcome by sensory experience. The loss of barrel organization and the lack of a precise functional map persisted in adult Th^{Kir} mice, as indicated by vGlut2 staining and the unrestrained cortical activation of cFos (Fig. 4E and fig. S15). The thalamus of Th^{Kir} mice retained a normal functional topography when whiskers were stimulated (Fig. 4F). Hence, the natural period of somatosensory-driven plasticity cannot overcome the altered organization that occurs in the embryo.

Our data reveals that embryonic patterns of thalamic activity organize the architecture of the somatosensory map. We show that the development of this map involves the emergence of functional cortical columns in embryos, driven by spontaneous thalamic wave-like activity. These embryonic columns display spatial segregation and somatotopic organization, despite the immature state of the cortical sheet in which they materialize. We propose that patterned activity in pre-cortical relay stations during embryonic stages prepares cortical areas and circuits for upcoming sensory input. As thalamic waves are not exclusive to the somatosensory nucleus but propagate to other sensory nuclei (e.g., visual or auditory (10)), the principles of cortical map organization described here might be common to other developing sensory systems.

Europe PMC Funders Author Manuscripts

Supplementary Material

Refer to Web version on PubMed Central for supplementary material.

Acknowledgments

We thank L.M. Rodríguez, R. Susín and B. Andrés for technical support; T. Iwasato for providing the TCA-GFP mouse, and A. Barco for advice on the behavioral experiments. R. Morris, S. Tole, M. Maravall and D. Jabaudon for critical reading of the manuscript, and the López-Bendito's laboratory for stimulating discussions.

Funding

Supported by grants from the European Research Council (ERC-2014-CoG-647012) and the Spanish Ministry of Science, Innovation and Universities (BFU2015-64432-R and Severo Ochoa Grant SEV-2017-0723). N.A-B held a FPI fellowship from the MINECO. H.G held postdoc fellowships from the Swedish Research Council and the Swedish Brain Foundation.

Data and materials availability

All the data in the paper are presented in the main text or supplementary materials.

References and Notes

1. Mountcastle VB. J Neurophysiol. 1957; 20:408–434. [PubMed: 13439410]
2. Rakic P. Science. 1988; 241:170–176. [PubMed: 3291116]
3. Hubel DH, Wiesel TN. J Physiol. 1962; 160:106–154. [PubMed: 14449617]
4. Rakic P, Ayoub AE, Breunig JJ, Dominguez MH. Trends Neurosci. 2009; 32:291–301. [PubMed: 19380167]
5. Tiriac A, Smith BE, Feller MB. Neuron. 2018
6. Hensch TK. Annu Rev Neurosci. 2004; 27:549–579. [PubMed: 15217343]
7. Gaspar P, Renier N. Curr Opin Neurobiol. 2018; 53:43–49. [PubMed: 29753205]
8. Killackey HP, Belford G, Ryugo R, Ryugo DK. Brain Res. 1976; 104:309–315. [PubMed: 1260427]
9. Woolsey TA, Wann JR. J Comp Neurol. 1976; 170:53–66. [PubMed: 977815]
10. Moreno-Juan V, et al. Nat Commun. 2017; 8 14172 [PubMed: 28155854]
11. Woolsey TA, Van der Loos H. Brain Res. 1970; 17:205–242. [PubMed: 4904874]
12. Agmon A, Yang LT, Jones EG, O'Dowd DK. J Neurosci. 1995; 15:549–561. [PubMed: 7823163]
13. Yang JW, et al. Cereb Cortex. 2013; 23:1299–1316. [PubMed: 22593243]
14. Mizuno H, et al. Cell Rep. 2018; 22:123–135. [PubMed: 29298415]
15. Mitrukhina O, Suchkov D, Khazipov R, Minlebaev M. Cereb Cortex. 2015; 25:3458–3467. [PubMed: 25100857]
16. Alagem N, Dvir M, Reuveny E. J Physiol. 2001; 534:381–393. [PubMed: 11454958]
17. Wagner J, Luhmann HJ. Neuropharmacology. 2006; 51:848–857. [PubMed: 16876205]
18. Calderon DP, Leverkova N, Peinado A. J Neurosci. 2005; 25:1737–1749. [PubMed: 15716410]
19. Mizuno H, et al. Neuron. 2014; 82:365–379. [PubMed: 24685175]
20. Erzurumlu RS, Gaspar P. Eur J Neurosci. 2012; 35:1540–1553. [PubMed: 22607000]
21. Li H, et al. Neuron. 2013; 79:970–986. [PubMed: 24012009]
22. Narboux-Neme N, et al. Journal of Neuroscience. 2012; 32:6183–6196. [PubMed: 22553025]
23. Van der Loos H, Woolsey TA. Science. 1973; 179:395–398. [PubMed: 4682966]
24. Weller WL, Johnson JI. Brain Res. 1975; 83:504–508. [PubMed: 1111817]
25. Lokmane L, Garel S. Semin Cell Dev Biol. 2014; 35:147–155. [PubMed: 25020201]
26. Crair MC, Malenka RC. Nature. 1995; 375:325–328. [PubMed: 7753197]
27. Gorski JA, et al. J Neurosci. 2002; 22:6309–6314. [PubMed: 12151506]

28. Chen L, Guo Q, Li J. Development. 2009; 136:1317–1326. [PubMed: 19279136]
29. Franco SJ, et al. Science. 2012; 337:746–749. [PubMed: 22879516]
30. Dupont E, Hanganu IL, Kilb W, Hirsch S, Luhmann HJ. Nature. 2006; 439:79–83. [PubMed: 16327778]
31. Curran-Everett D. Am J Physiol Regul Integr Comp Physiol. 2000; 279:R1–8. [PubMed: 10896857]

Europe PMC Funders Author Manuscripts

Europe PMC Funders Author Manuscripts

One Sentence Summary

Mapping of touch sensation into brain regions is driven prenatally by spontaneous brain activity.

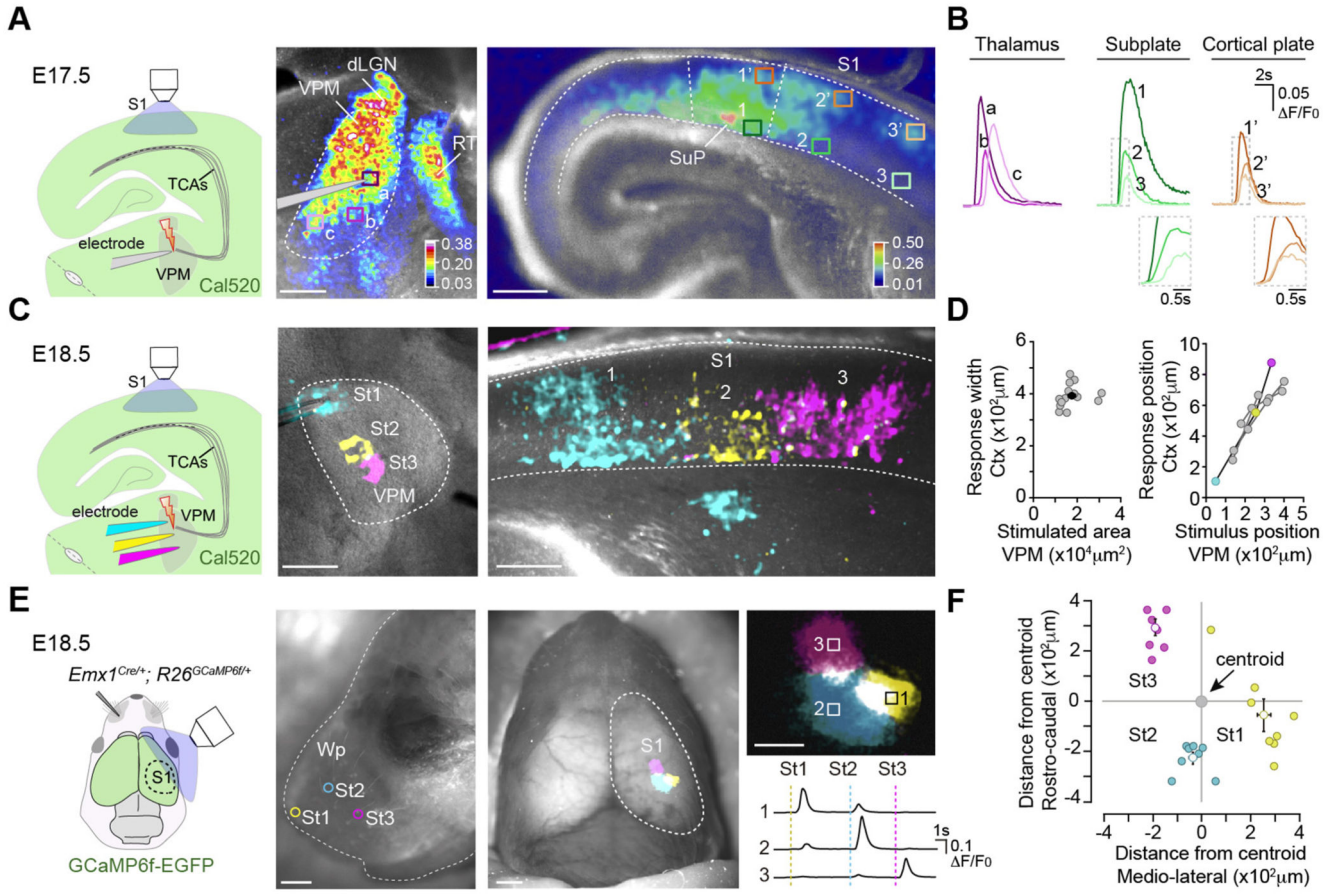

Fig.1. Embryonic thalamocortical stimulation reveals an organized prenatal cortical map.

(**A**) Experimental design. Maximal projection of the calcium responses ($\Delta F/F_0$, color coded) in the ventral postero-medial nucleus (VPM) and cortex after VPM stimulation at E17.5. (**B**) Calcium transients from boxes in A. (**C**) Experimental design. Maximal projection of cortical responses after stimulation of three adjacent VPM regions at E18.5. (**D**) Plot of stimulated VPM area versus cortical response width (black dot equals mean value). Right: Plot of the stimulus position in the VPM versus the cortical response location ($n = 16$). Colored circles represent the data in C. (**E**) Experimental design. Cortical calcium responses elicited by mechanical stimulation of three contralateral whisker pad (Wp) sites (St1-St3) at E18.5. Right: High-magnification and transients recorded in each ROI (boxes 1-3). (**F**) Plot of the position of each cortical response relative to the centroid of the activated area ($n = 8$). dLGN, dorso-lateral geniculate nucleus; RT, reticular thalamus; SuP, subplate; TCAs, thalamocortical axons. Scale bars, 200 μm in **A**; 1 mm in **E** (left/middle) and 500 μm in **E** (right).

Europe PMC Funders Author Manuscripts

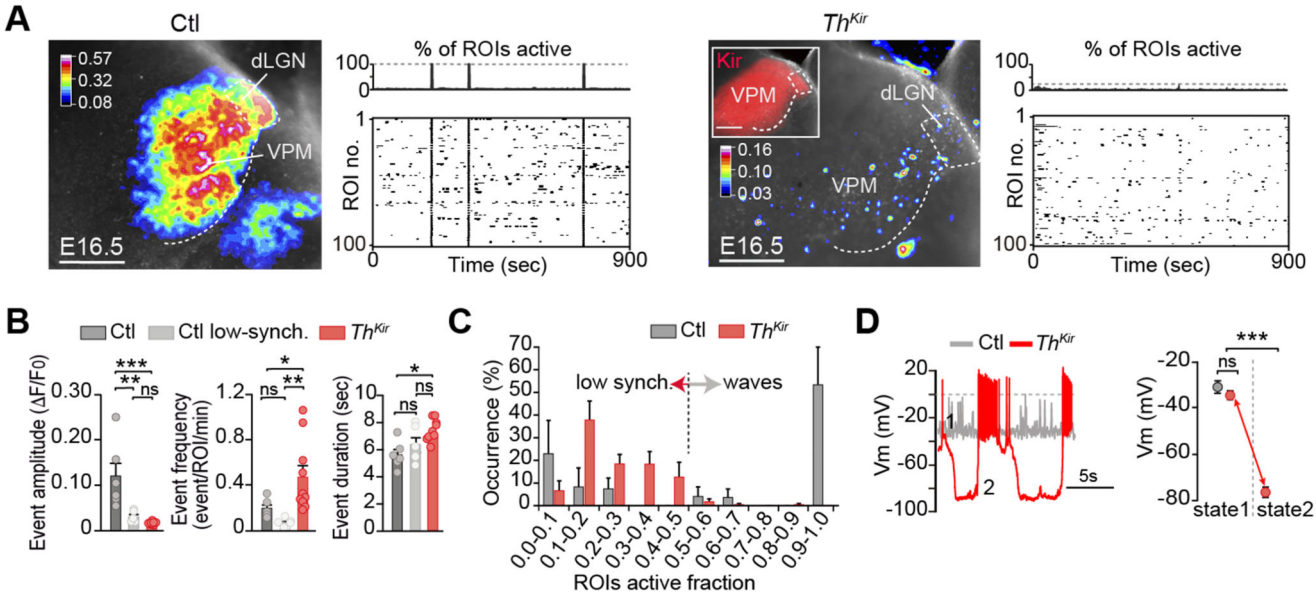

Fig.2. Desynchronizing the embryonic thalamic pattern of activity.

(**A**) Maximal projection of *ex vivo* spontaneous calcium activity in the ventral postero-medial nucleus (VPM) and accompanying raster plots in control and Th^{Kir} slices at E16.5. (**B**) Properties of the VPM calcium events ($n = 6$ control, $n = 10$ Th^{Kir}; $*P < 0.05$, $**P < 0.01$, $***P < 0.001$). (**C**) Percentage distribution of active ROIs. (**D**) Representative traces and quantification of membrane potential (Vm) in control and Th^{Kir} neurons recorded at E16.5-E18.5 (control $n = 7$; Th^{Kir} $n = 7$). $***P < 0.001$. dLGN, dorso-lateral geniculate nucleus. Scale bars, 200 μm. Data are means ± SEM.

Europe PMC Funders Author Manuscripts

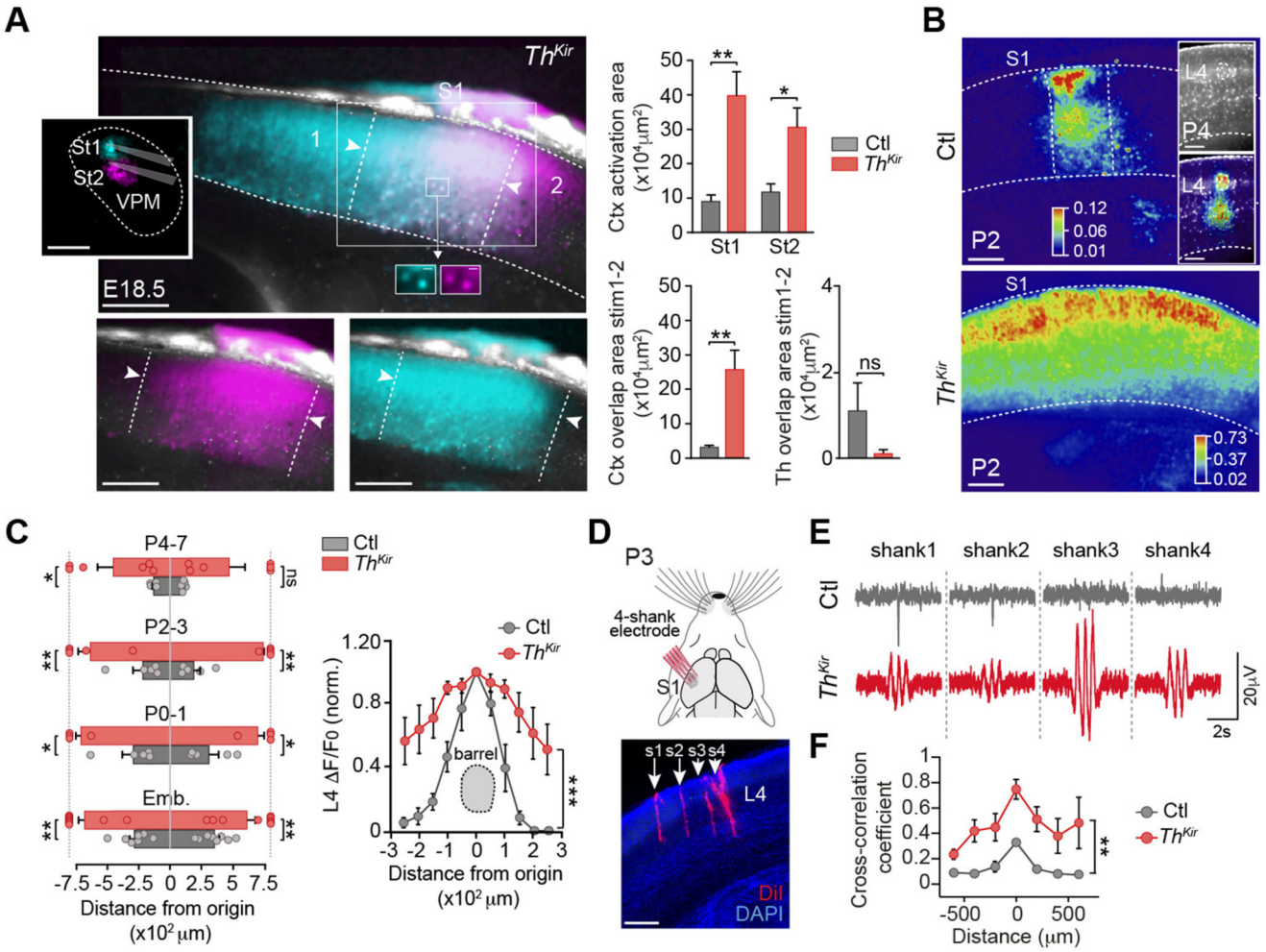

Fig.3. Loss of functional cortical pre-barrel columns in the *Th^Kir^* mice.

(**A**) Maximal projection of cortical responses after stimulation of two adjacent ventral postero-medial (VPM) regions in *Th^Kir^* slices. Right: Quantifications of the activated area (n = 6 control, n = 6 *Th^Kir^*; *P < 0.05, **P < 0.01). (**B**) Cortical activation elicited by VPM stimulation at P2 (inset: P4) in control and *Th^Kir^* slices. (**C**) Quantification of the horizontal spread of the cortical response (E17-18 n = 8 control, n = 9 *Th^Kir^*; P0-1 n = 5 control, n = 4 *Th^Kir^*; P2-3 n = 5 control, n = 5 *Th^Kir^*; P4-7 n = 5 control, n = 6 *Th^Kir^*). Right: Same in layer 4 at P4-P7 (n = 6 control, n = 6 *Th^Kir^*; ***P < 0.001). (**D**) Experimental design and coronal image showing the 4-shank (s1-s4) electrode insertion in S? (red). (**E**) Representative *in vivo* recordings of spontaneous cortical network activity. (**F**) Quantification of the cross-correlation coefficient among shanks in control (n = 3) and *Th^Kir^* mice (n = 6). **P < 0.01. Scale bars, 200 µm. Data are means ± SEM.

Europe PMC Funders Author Manuscripts

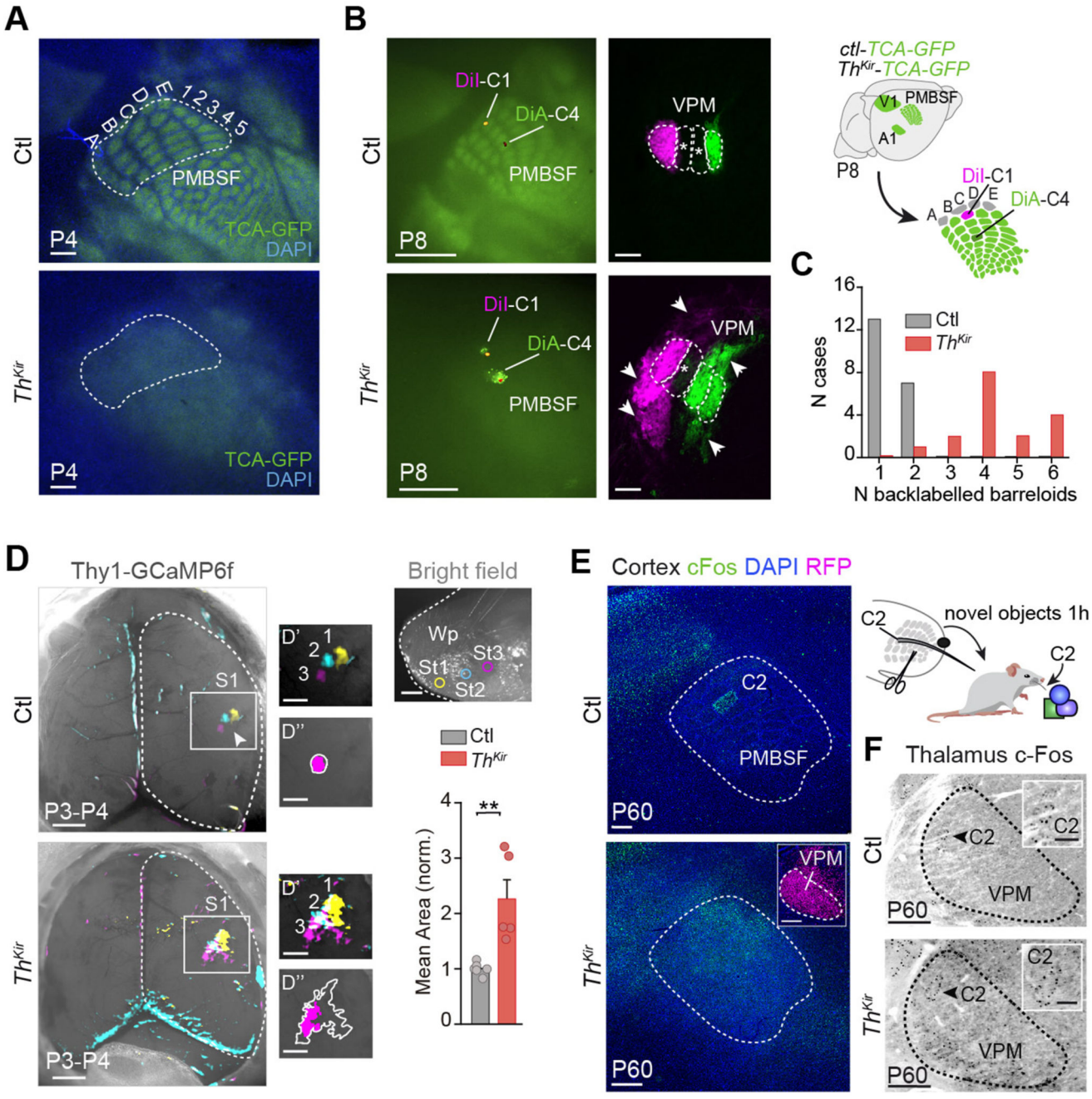

Fig.4. Long-term anatomical and functional changes in S1 of the *Th*^{Kir} mice.

(**A**) Tangential sections showing the postero-medial barrel subfield (PMBSF) in control and *Th*^{Kir} TCA-GFP mice at P4. (**B**) Experimental design and images showing PMBSF injection sites and back-labeled barreloids in the ventral postero-medial nucleus (VPM). (**C**) Quantification of data shown in B ($n = 10$ control, $n = 10$ *Th*^{Kir}). (**D**) Maximal projection of the *in vivo* contralateral cortical responses elicited by mechanical stimulation of three whisker pad (Wp) sites at P3-P4 (top right). D': high-power views. D": drawing of initial (pink) and maximal (outline) extension of representative responses. Bottom-right:

Quantification of the data ($n = 6$ control, $n = 5$ Th^{Kir}; $^{**}P < 0.01$). (**E**) Experimental design and cortical cFos immunostaining. (**F**) VPM cFos immunostaining. Scale bars, 300 μm in **A, B** right, **E** and **F** (insets 100 μm); 1 mm in **B** left and **D** (insets 500 μm). Data are means ± SEM.

Europe PMC Funders Author Manuscripts